POLITECNICO DI TORINO
Repository ISTITUZIONALE

Multiobjective optimization of a cable-driven robot for wrist rehabilitation using a genetic algorithm

(Article begins on next page)

16 May 2024

MULTIOBJECTIVE OPTIMIZATION OF A CABLE-DRIVEN ROBOT FOR WRIST REHABILITATION USING A GENETIC ALGORITHM

ANDREA BOTTA

Department of Mechanical Engineering, Tokyo Institute of Technology, Japan,
Department of Mechanical and Aerospace Engineering, Politecnico di Torino, Italy
andrea.botta@polito.it

GIUSEPPE QUAGLIA

Department of Mechanical and Aerospace Engineering, Politecnico di Torino, Italy,
giuseppe.quaglia@polito.it

YUKIO TAKEDA

Department of Mechanical Engineering, Tokyo Institute of Technology, Japan,
takeda.y.aa@m.titech.ac.jp

ABSTRACT
This paper presents a multi-objective optimization using a genetic algorithm to reduce the size of the current configuration of a cable-driven end-effector robot for wrist rehabilitation. The objective of this work is to obtain a smaller robot with good performance by employing a constrained genetic algorithm (GA) so the device can be light and wearable. The optimization was performed to study the effect of the robot dimensions and in the end, a new solution that can reduce the robot size by 35% and increase the performance by 1.8% was found.

KEY WORDS: SDG 3, Assistive Robotics, Cable-Driven Robot, Wrist Rehabilitation, Medical Devices, Genetic Algorithm Optimization

1. INTRODUCTION

The lack of specialized personnel and assistive technology to assist in rehabilitation therapies is one of the challenges facing the health sector today, and it is projected to increase as the global population ages [1]. Among the different types of injuries, hand injuries occur most frequently [2]. These injuries require a long and repetitive rehabilitation process for the hand to regain its functionality [3].

To support the lack of therapists, several robotic rehabilitation devices have been proposed recently. Kwakkel *et al.* [4] reported on the effectiveness of robotic rehabilitation with clinical trials. Hussain *et al.* [5] presented many robotic devices for wrist rehabilitation and also provide the exoskeleton/end-effector classification. Exoskeleton robots [6–8] are made of a kinematic chain that mimics the actual human kinematic chain and its joints. For this reason, particular care must be placed on avoiding robot-human joint misalignment to avoid hurting the user [9]. On the other hand, end-effector rehabilitation robots don't match the human kinematic chain but simply apply the required forces and torques [10, 11]. Thus, there are no problems related to joint misalignment but for the same reason force application must be properly controlled to not damage the joints with unfeasible motions [5].

In response to these critical issues, this research proposes the development of RehaWrist.q, a 3 degree of freedom (DoF) cable-guided end-effector system that is also wearable, compact, lightweight, and does not require external support.

2. WRIST KINESIOLOGY

The human wrist is a 2 DoFs joint that links the hand to the forearm, enabling flexion-extension (FE) β (Fig. 1a) and radial-ulnar deviation (RUD) γ (Fig. 1b) motions. Moreover, there is an additional motion named pronation-supination (PS) α (Fig. 1c) that is usually considered useful for rehabilitation although it is produced by a joint between the forearm and the elbow.
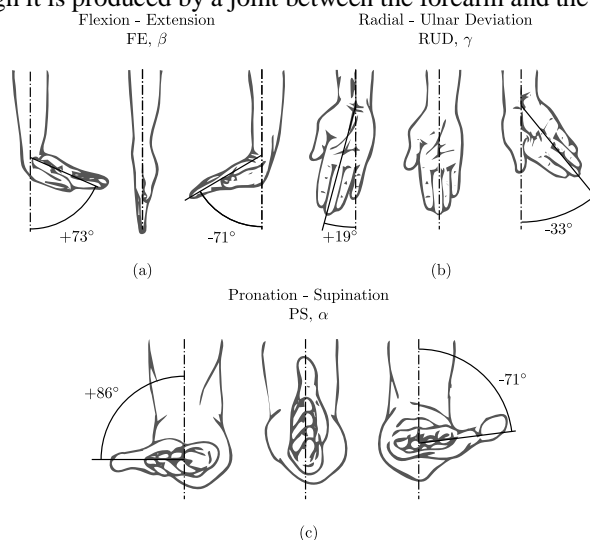

Fig. 1 Wrist motions and their maximum range of motions [12]

3. PROPOSED REHABILITATION ROBOT

In the following section, the functional design of the robot is presented and then a new performance index based on the robot's dimensions is introduced.

3.1 Functional Design

Fig. 2a depicts the functional design of RehaWrist.q. The device is composed of two platforms: the fixed platform is integral with a brace-like structure that is worn on the upper arm, and the mobile platform moves together with the user's hand thanks to a handle or a glove. The two platforms have a width of $2L_0$ and $2L_1$, respectively. Also, the fixed one is placed at a distance d_0 from the centre of the wrist O_W whereas the mobile one is at d_1 from the same point but in the opposite direction (Fig. 2b). A revolute joint between the fixed platform and the forearm enables the PS motion. The two platforms are connected by four actuated cables to control the mobile platform pose. By properly tensioning the cables it is possible to achieve one of the three rehabilitation motions or a combination of them. For example, a radial deviation motion ($\gamma > 0$) occurs by pulling cables $\mathbf{p}_1 = A_0A_1$ and $\mathbf{p}_2 = B_0A_1$. An ulnar deviation motion ($\gamma < 0$) is obtained by pulling cables $\mathbf{p}_3 = A_0B_1$ and $\mathbf{p}_4 = B_0B_1$. Similarly, the pairs $\mathbf{p}_1$ and $\mathbf{p}_3$ or $\mathbf{p}_2$ and $\mathbf{p}_4$ control the FE motion while the pairs $\mathbf{p}_1$ and $\mathbf{p}_4$ or $\mathbf{p}_2$ and $\mathbf{p}_3$ drive the PS motion.
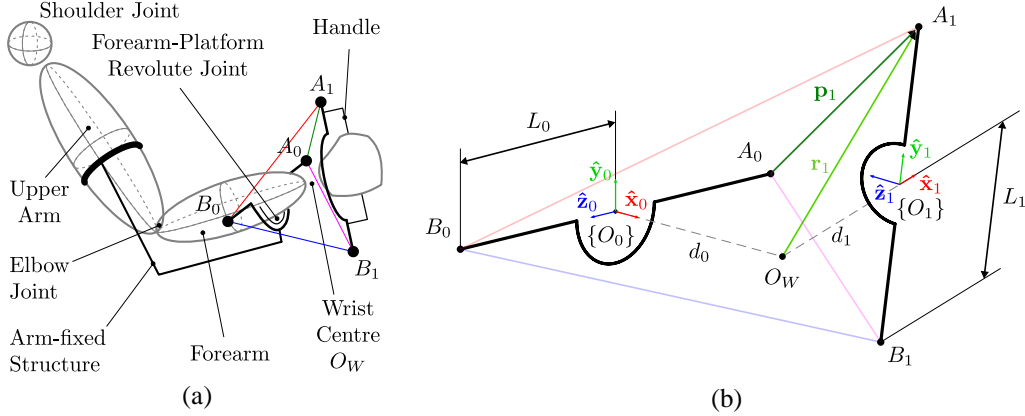
Fig. 2 (a) Functional diagram of the rehabilitation robot. (b) Schematic representation of RehaWrist.q in a generic pose. Only the vectors related to cable 1 are shown.

3.2 Transmission Index

In a previous work [13], the authors defined a dimensionless index named transmission index to evaluate the efficiency of cable-driven robots. The transmission index τ_{ai} measure how much of the total tension applied to the cable $i = 1, \dots, 4$ produces a useful torque about the generic $\hat{\mathbf{a}}$ axis of rotation. It is defined as

$$\tau_{ai} = \frac{\hat{\mathbf{p}}_i \cdot (\hat{\mathbf{r}}_i \times \hat{\mathbf{a}})}{|\hat{\mathbf{p}}_i|} = \hat{\mathbf{p}}_i \cdot (\hat{\mathbf{r}}_i \times \hat{\mathbf{a}})$$

where $\hat{\mathbf{p}}_i \cdot (\hat{\mathbf{r}}_i \times \hat{\mathbf{a}})$ is the projection of the i-th cable direction along the most effective direction to generate a torque about the generic $\hat{\mathbf{a}}$ axis.

In the case of the PS motion, the end-effector rotates about $\hat{\mathbf{x}}_1$, therefore $\tau_{xi} = \hat{\mathbf{p}}_i \cdot \hat{\mathbf{z}}_1$. Similarly, in the case of FE motion the rotation axis is $\hat{\mathbf{y}}_1$ and $\tau_{yi} = \hat{\mathbf{p}}_i \cdot \hat{\mathbf{z}}_1$. Both rotations have the same effective direction, $\hat{\mathbf{z}}_1$, but different lever arms. The case of RUD is completely different as the rotation axis is $\hat{\mathbf{z}}_1$ and the transmission index is $\tau_{zi} = \hat{\mathbf{p}}_i \cdot (\hat{\mathbf{r}}_i \times \hat{\mathbf{z}}_1)$.

3.3 Current Design

The transmission index τ_{ai} only depends on the robot's proportions. Hence it is possible to design the robot by means of τ_{xi}, τ_{yi} and τ_{zi}. The authors in [13] presented in depth the methodology to define the robot proportions using the transmission index and dimensionless parameters representing the robot size. In the paper three solutions were found without using any optimization approach and among them one was considered promising (Table 1).

Table 1 Current design proportions obtained in [13]

d_0	d_1	L_0	L_1
60 mm	20 mm	160 mm	100 mm

Although this configuration showed to be promising in terms of τ_{ai} it clearly presents some flaws, in particular when size is taken into consideration. L_0 is quite large and this doesn't go well with the idea of having a compact wearable device. Moreover, d_1 could be larger since it affects the lever arm of the cable force during FE and RUD motions.

4. ROBOT DESIGN OPTIMIZATION

Since the first robot configuration could not be optimal, this paper aims at finding better solutions by employing a proper multi-objectives optimization to define a trade-off configuration with high transmission indexes but reduced size.

4.1 Methodology

To perform the robot design optimization a multi-objective constrained genetic algorithm (GA) was used. In particular, the *gamultiobj* function defined in Matlab was used. An initial population of 1500 individuals was used, a crossover fraction of 0.8 was set and the default mutation function was employed. The objectives were to maximize the average value of τ_{a1} in the respective range of motion and minimizing the sum of $dim = L_0 + L_1$ by finding the best value of d_0, d_1, L_0, and L_1. Since the GA always find to minimize the fitness function, the first objective is re-defined as minimizing the average value of $-\tau_{a1}$. Note that only cable 1 is considered because, depending on the motion, one of the other cables behaves in the same way while the other two have a symmetrical behaviour. Also, only L_0 and L_1 were considered when computing the size of the robot. Table 2 collects the relevant details for each optimization problem. In the following, the objective 1 is also called Transmision Index (TI) Score and the objective 2 is also named Size Score.

Table 2 Design optimization problems

	min Objective 1	min Objective 2	Range of Motion
PS Optimization	$\mathrm{avg}(-\tau_{x1})$	$dim = L_0 + L_1$	$\alpha = \pm 60°$
FE Optimization	$\mathrm{avg}(-\tau_{y1})$	$dim = L_0 + L_1$	$\beta = \pm 60°$
RUD Optimization	$\mathrm{avg}(-\tau_{z1})$	$dim = L_0 + L_1$	$\gamma = \pm 33°$
3 DoFs Optimization	$\mathrm{avg}(-\tau_{x1}) + \mathrm{avg}(-\tau_{y1}) + \mathrm{avg}(-\tau_{z1})$	$dim = L_0 + L_1$	α, β, γ

The parameters set was constrained by upper and lower bounds as shown in Table 3. The lower bound of d_1 was set to 50 mm to favor configurations with larger d_1 since it affects the lever arms of the cable during FE and RUD motions.

Table 3 Size parameter upper and lower bounds

	d_0 [mm]	d_1 [mm]	L_0 [mm]	L_1 [mm]
Lower bound	10	50	50	50
Upper bound	200	150	300	300

4.2 Results

Figure Fig. 3 reports the results of the GA optimization considering only one of the three motions at a time. For each optimization, the resulting Pareto front is shown together with the current configuration fitness. The highlighted area represents all possible solutions that present a larger transmission index than the current solution and a smaller size than the current solution. All the points on the Pareto front and within the highlighted area are optimal solutions.

The PS and FE cases (Fig. 3a-b) are very similar since both of them have the same transmission index $\tau_{xi} = \tau_{yi} = \hat{\mathbf{p}}_i \cdot \hat{\mathbf{z}}_1$, so they can be optimized together. For both of them, the GA optimization shows that there is room for improving both the efficiency (τ_{ai}) and the size compared to the current configuration. In particular, the transmission index for these two motions favours larger L_0 while the other parameters stay close to their lower bounds. The larger is L_0, the higher are τ_{xi} and τ_{yi}. Since size is of the utter importance, the configuration on the Pareto front (i.e., the set of most optimal configurations considering both objectives at the same time) with the same τ_{ai} of the current solution is considered the best trade-off between size and performance. Such configuration is defined by the following parameters: $d_0 = 10\,\text{mm}$, $d_1 = 50\,\text{mm}$, $L_0 = 105$ mm, and $L_1 = 50$ mm.

The RUD case is completely different from the other two. The current solution was not optimized for this motion as shown by the optimization results in Fig. 3c: any configuration on the Pareto front is better both in size and efficiency. However, it is interesting to notice that RUD motion can not achieve the same level of performance as the other two with the previously defined constraints. Looking at the optimized configurations produced by the GA, all of them tend to maximize d_0 and keeping the other parameters closer to their lower bounds. The second parameter that influences performance is L_1 because it improves performance by becoming larger but it is kept at a reasonable size by the minimization of the size. On the other hand, d_0 doesn't influence the size score, thus for all configurations, it is equal to 200 mm. Such design may be feasible in term of size and performance, but with such proportions, the risk of interference between the cables and the forearm is extremely high and the resulting range of motions are reduced.
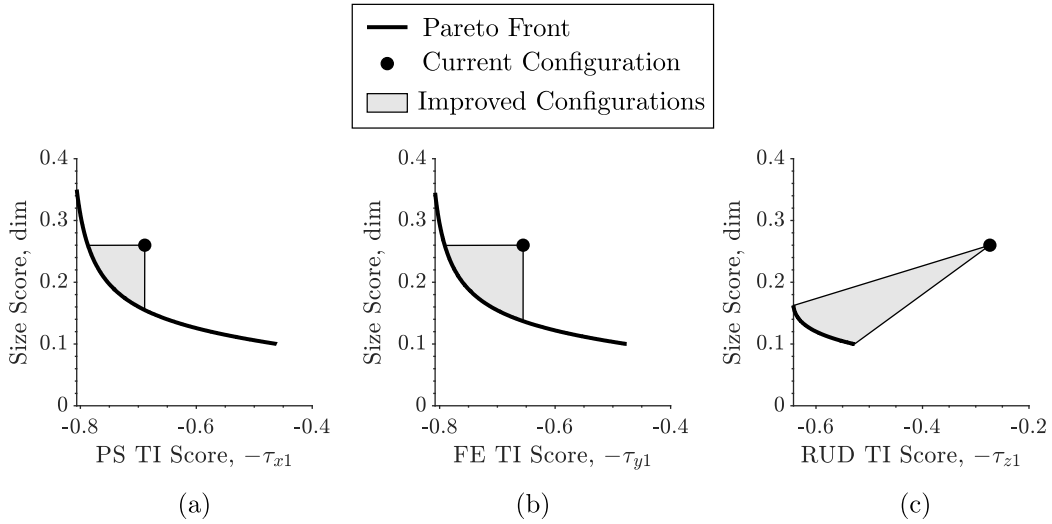

Fig. 3 Result of the GA optimization considering the transmission index of a single motion and the size of the robot

Since the RUD motion requires completely different proportions than the other two motions, it is interesting to optimize the robot proportions considering all motions together. Fig. 4 illustrates the results of such GA optimization in two different cases. In Fig. 4a, the same upper bounds constraint as the other optimization was used. In Fig. 4b, the upper bounds of L_0 and L_1 were

reduced to 120 mm to force a smaller robot but at the same time the lower bound of d_1 was reduced to 25 mm to improve the transmission indexs. In the first case, the current configuration is quite close to the Pareto front found by the GA, thus only minimal improvements can be achieved. If the configuration with the smallest size and the same transmission index as the current solution is considered, the robot would have the following dimensions $d_0 = 47\,\text{mm}$, $d_1 = 50\,\text{mm}$, $L_0 = 189\,\text{mm}$, and $L_1 = 50\,\text{mm}$. Such proportions result in an even larger L_0 than the original configuration thanks to the reduced L_1 dimension. Thus, all improved configurations are practically larger than the current ones.

For that reason and because the objective of this paper is to obtain a smaller robot with good performance, the GA optimization was performed with a stricter upper bound for L_0 and L_1 (120 mm). The optimization result in Fig. 4b clearly shows that this new optimization is able to produce significantly smaller proportions and a slight performance improvement. By taking into consideration the point on the Pareto Front with better combined transmission index score, the robot proportions are $d_0 = 59\,\text{mm}$, $d_1 = 25\,\text{mm}$, $L_0 = 120\,\text{mm}$, and $L_1 = 50\,\text{mm}$. This particular solution can reduce the robot size by 35% and increase the overall TI Score by 1.8%.
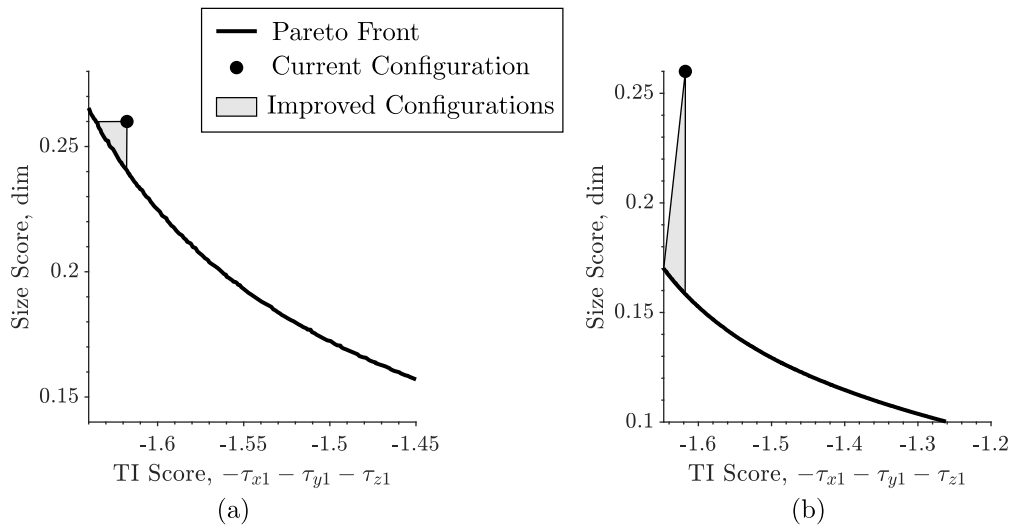

Fig. 4 Result of the GA optimization considering the transmission index of all motions and the size of the robot. (a) Parameters upper bounds = [200 150 300 300] mm. (b) Parameters lower bounds = [10 25 50 50] mm and upper bounds = [200 150 120 120] mm.

Fig. 5 depicts the detail of the individual transmission indices for the current configuration and the one found with the GA. The PS motion has a slightly lower transmission index for half of the range of motion while it is practically the same for the other half. The FE motion shows an improvement when the mobile platform is pulled toward the fixed one. For the other half of the range of motion, the transmission index is very similar to the current one. The RUD motion presents an improvement across the whole range of motion.
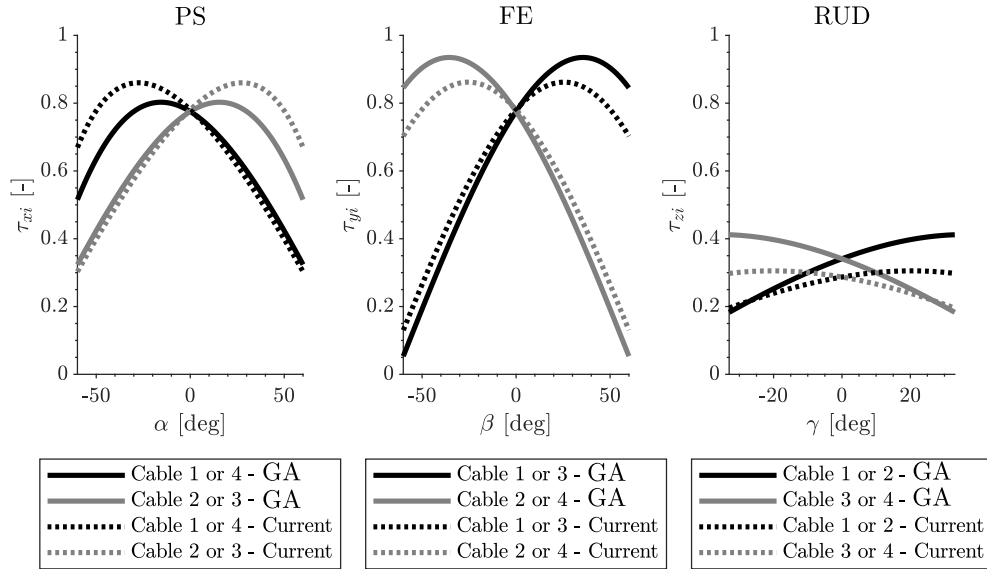
Fig. 5 Comparison of the transmission indices of the robot in the current configuration and in the configuration obtained with the GA.

5. CONCLUSIONS

This work presented a multi-objective optimization using a genetic algorithm to reduce the size of the current configuration of the proposed cable-driven robot for rehabilitation. To achieve that, first the transmission indexes for each motion were defined to quantify the performance of the robot based only on its proportions. Then an objective related to the robot dimensions was defined. Given these quantities, it was possible to carry on a series of optimization for the individual motions and for their combination. In the end, a new and smaller configuration was found that slightly increase the performance indices of the original configuration

REFERENCES

1. Marć M, Bartosiewicz A, Burzyńska J, Chmiel Z, Januszewicz P (2019) A nursing shortage – a prospect of global and local policies. International Nursing Review 66:9–16

2. Crowe CS, Massenburg BB, Morrison SD, et al (2020) Global trends of hand and wrist trauma: a systematic analysis of fracture and digit amputation using the Global Burden of Disease 2017 Study. Injury Prevention 26:i115–i124

3. Albanese GA, Marini F, Taglione E, et al (2019) Assessment of human wrist rigidity and pain in post-traumatic patients. In: 2019 IEEE 16th International Conference on Rehabilitation Robotics (ICORR). pp 89–94

4. Kwakkel G, Kollen BJ, Krebs HI (2008) Effects of Robot-Assisted Therapy on Upper Limb Recovery After Stroke: A Systematic Review. Neurorehabil Neural Repair 22:111–121

5. Hussain S, Jamwal PK, Van Vliet P, Ghayesh MH (2020) State-of-the-Art Robotic Devices for Wrist Rehabilitation: Design and Control Aspects. IEEE Transactions on Human-Machine Systems 50:361–372

6. Su Y-Y, Yu Y-L, Lin C-H, Lan C-C (2019) A compact wrist rehabilitation robot with accurate force/stiffness control and misalignment adaptation. Int J Intell Robot Appl 3:45–58

7. Liu Y-C, Takeda Y (2020) Kineto-Static Analysis of a Wrist Rehabilitation Robot with Compliance and Passive Joints for Joint Misalignment Compensation. Machines 8:23

8. Liu Y-C, Botta A, Quaglia G, Takeda Y (2022) Preliminary Mechanical Design of a Wearable Parallel-Serial Hybrid Robot for Wrist and Forearm Rehabilitation with Consideration of Joint Misalignment Compensation. In: ROMANSY 24 - Robot Design, Dynamics and Control Proceedings of the 24th CISM IFToMM Symposium. Springer, Singapore, pp 53–61

9. Näf MB, Junius K, Rossini M, Rodriguez-Guerrero C, Vanderborght B, Lefeber D (2019) Misalignment Compensation for Full Human-Exoskeleton Kinematic Compatibility: State of the Art and Evaluation. Applied Mechanics Reviews. https://doi.org/10.1115/1.4042523

10. Gonçalves RS, Brito LSF, Moraes LP, Carbone G, Ceccarelli M (2020) A fairly simple mechatronic device for training human wrist motion. International Journal of Advanced Robotic Systems 17:1729881420974286

11. Shi K, Song A, Li Y, Li H, Chen D, Zhu L (2021) A Cable-Driven Three-DOF Wrist Rehabilitation Exoskeleton With Improved Performance. Frontiers in Neurorobotics 15:

12. MD IAK (2007) The Physiology of the Joints, Volume 1: Upper Limb, Volume 1, 5th edition. Churchill Livingstone, Edinburgh

13. Colucci G, Botta A, Verutti M, Visconte C, Quaglia G, Liu Y-C, Takeda Y (2022) A preliminary synthesis of a light and compact wearable cable-driven parallel robot for wrist joint rehabilitation. In: Proceedings of Jc-IFToMM International Symposium. Kyoto, Japan, pp 57–64